Design of polarization-insensitive components using geometrical and stress-induced birefringence in SOI waveguides

D.-X. Xu, W. N. Ye, A. Bogdanov, D. Dalacu, A. Delâge, P. Cheben,
S. Janz, B. Lamontagne, M.-J. Picard

Institute for Microstructural Sciences, National Research Council Canada (NRC),
Ottawa, Ontario, Canada, K1A 0R6

ABSTRACT

We review the use of the oxide cladding stress induced photoelastic effect to eliminate the modal birefringence in silicon-on-insulator (SOI) ridge waveguide components, and highlight characteristics particular to high index contrast (HIC) systems. The birefringence in planar waveguides has its origin in the electromagnetic boundary conditions at the waveguide boundaries, and can be further modified by the presence of stress in the materials. It is shown that geometrical constraints imposed by different design and fabrication considerations become increasingly difficult to satisfy with decreasing core sizes. On the other hand, with typical stress levels of -100 MPa to -400 MPa (compressive) in SiO_2 used as the upper cladding, the effective indices are altered up to the order of 10^{-3} for ridges with heights ranging from 1 μm to 5 μm. We demonstrate that the stress can be effectively used to balance the geometrical birefringence. Birefringence-free operation is achieved for waveguides with otherwise large birefringence by using properly chosen thickness and stress of the upper cladding layer. This allows the waveguide cross-section profiles to be optimized for design criteria other than zero-birefringence. Since the index changes induced by the stress are orders of magnitude smaller than the waveguide core/cladding index contrast, changes in the mode profiles are insignificant and the associated mode mismatch loss is negligible. We study the stress-induced effects in two parallel waveguides of varying spacing, to emulate the condition in directional couplers and ring-resonators. In the arrayed waveguide grating (AWG) demultiplexers fabricated in the SOI platform, we demonstrated the reduction of the birefringence from 1.3×10^{-3} (without the upper cladding) to below 1×10^{-4} across the spectral band by using a 0.6 μm oxide upper cladding with a stress of -320 MPa (compressive). Design options for relaxed dimensional tolerance and improved coupler performance made available by using stress engineering are discussed.

Keywords: polarization, birefringence, silicon-on-insulator (SOI), waveguides, stress, strain, arrayed waveguide gratings (AWG), directional coupler, ring resonator

1. INTRODUCTION

Silicon-on-insulator (SOI) offers several attractive features as a photonic material. It is gaining wider acceptance, with several significant advances achieved in recent years.[1-7] The earlier implementation of SOI devices mainly focused on relatively large core size devices (≥ 5 μm), driven by considerations such as an acceptable coupling efficiency between fibers and the waveguides.[6, 7] At the other end of the spectrum, SOI has been used to produce photonic crystals and Si nano-wire waveguides, where the silicon thickness is generally less than 0.5 μm.[1, 8] By reducing the core size, waveguides with smaller bend radii can be adopted, and more compact devices can be implemented. Conventional ridge waveguide-based components can provide compact device foot-print, using relatively well understood optical design principles and standard fabrication technologies, and therefore offer near-term commercial potential. Application-oriented research has focused on reducing the core size in this range, down-scaling the devices and exploring the integrated optics potential of SOI.

There are certainly challenges in developing SOI-based microphotonics into a commercially viable technology. The fiber-waveguide coupling, propagation loss due to scattering, and polarization dependence are some of the key issues.[10] These same issues are manageable in devices of large core size (5-10 μm), but become increasingly challenging as the

Optoelectronic Integration on Silicon II, edited by
Joel A. Kubby, Ghassan E. Jabbour, Proceedings of SPIE Vol. 5730
(SPIE, Bellingham, WA, 2005) · 0277-786X/05/$15 · doi: 10.1117/12.589158

waveguide size is reduced. There is a broad effort to overcome these obstacles, and practical solutions are being invented.[11-16]

Birefringence is an important issue in integrated optical systems. In applications such as wavelength demultiplexing and high resolution spectroscopy, the birefringence must be of the order of 10^{-5} for acceptable polarization insensitive performance. The geometrical birefringence can be adjusted to zero for a specific aspect ratio (e.g. the ratio of ridge width and ridge etch depth).[6, 17-20] This method is successful for waveguides with relatively large cross-sections. However, as the waveguide size shrinks to 2 μm or below, the birefringence is highly sensitive to the fluctuations in the waveguide dimensions, and it can become very large. In a typical high index contrast SOI ridge waveguide with width and height approaching one micron, the birefringence can easily be larger than 10^{-3}. Furthermore, ridge dimensions also determine the number of waveguide modes, the minimum usable bend radius, the mode size, and the coupling between adjacent waveguides. It is often impossible to simultaneously meet several design objectives, including zero birefringence, by adjusting waveguide dimensions alone. These constraints have recently been investigated by several research groups.[18-20]

We have recently reported the significant effects of cladding stress-induced birefringence in SOI waveguides, and the utilization of these effects as added design tools.[16, 21, 22] Although photoelastic effect in solids was discovered more than a century ago, and it is an important topic in glass-based waveguide technology,[23, 24] the impact of this phenomenon in SOI waveguides has not been generally recognized.

In this paper, we review the characteristics of modal birefringence in SOI waveguides, with regard to the two main sources of polarization anisotropy, namely the geometrical and the stress-induced birefringence, in sections 3 and 4 respectively. Both rectangular and trapezoidal waveguide cross-sections are considered. The compressive stress present in an oxide upper cladding layer is used as the primary example, and we will demonstrate that a compressive stress is a preferred choice. Stress in other cladding materials is governed by the same principles. Experimental demonstrations of polarization compensation are presented in section 5, that validate the simulation results. How the stress-induced effect manifests itself in multiple waveguides is studied in section 6. The evolution of these effects with decreasing core size is discussed in section 7. In section 8 we offer a few examples of how to use stress-induced birefringence to facilitate the design of waveguide components.

2. PRESENCE OF UPPER CLADDING OXIDE: GEOMETRICAL EFFECTS

An upper cladding layer is often used in planar waveguides to reduce the influence of surface contamination or to provide electrical isolation. For SOI, this layer is often SiO_2, although nitride or polymers are also used in some cases. In this section we discuss the geometrical effects of an oxide upper cladding that is caused exclusively by the refractive index difference compared to an air upper cladding. The structures are slab waveguides as shown in Fig. 1(a), with an oxide upper cladding thickness t_c, and the lower cladding is assumed to be semi-infinite in the simulations.

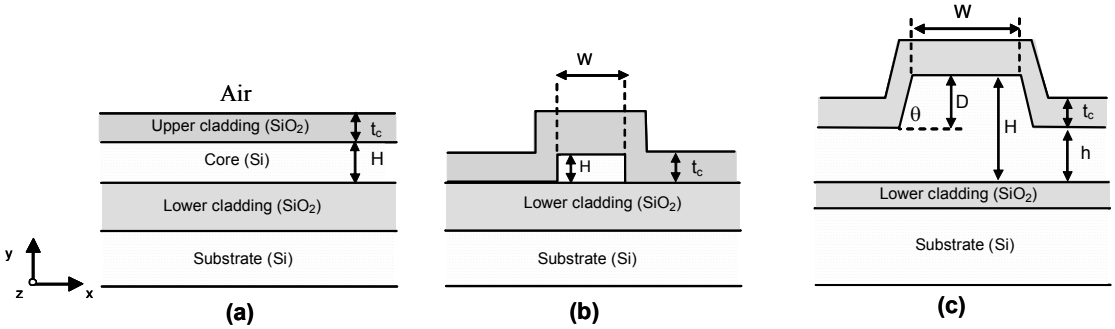

Fig. 1 Cross-section of SOI waveguides: (a) slab, (b) strip, and (c) ridge.

Shown in Fig. 2 are the modifications in the effective indices for the TE and TM modes in slab waveguides of thickness 0.5, 1 and 2 μm, respectively, with increasing oxide thickness t_c, calculated using the finite difference transfer matrix method. The n_{eff}^{TM} and n_{eff}^{TE} denote the effective indices of the TM (electrical field perpendicular to the wafer plane)

and TE (electrical field parallel to the wafer plane) modes, respectively. With the presence of oxide upper cladding, the index contrast is reduced from approximately 2.5 to 2, and the mode confinement is slightly reduced. A finite fraction of the optical intensity penetrates in the oxide, and both n_{eff}^{TM} and n_{eff}^{TE} become slightly higher. The TM mode is more strongly affected. For the Si thicknesses considered here, both n_{eff}^{TM} and n_{eff}^{TE} saturate for oxide thickness of 0.3 μm, with a maximum increase in n_{eff}^{TM} on the order of 10^{-2}. For thicker Si slab waveguides, a thinner layer of oxide is sufficient to fully contain the mode. Upon closer examination for thin oxide layers of thickness up to 10 nm (Fig. 2b), which is comparable to the thickness of native oxide, n_{eff}^{TM} and n_{eff}^{TE} increase with the oxide thickness t_c in an almost linear manner. Up to 10^{-3} of increase in n_{eff}^{TM} is observed. These values represent the lower limit for the effect of the oxide cladding. For ridges of various dimensions and aspect ratios, more surface area is exposed to the upper cladding and the mode is less confined, the effects is expected to be larger than that for slabs of similar thickness. Since the thickness of native oxide is difficult to control, this leads to added uncertainties in experiments. For this reason, we suggest that it is preferable to have sufficiently thick oxide (or another stable and transparent material) as the upper cladding to provide well controlled mode properties.

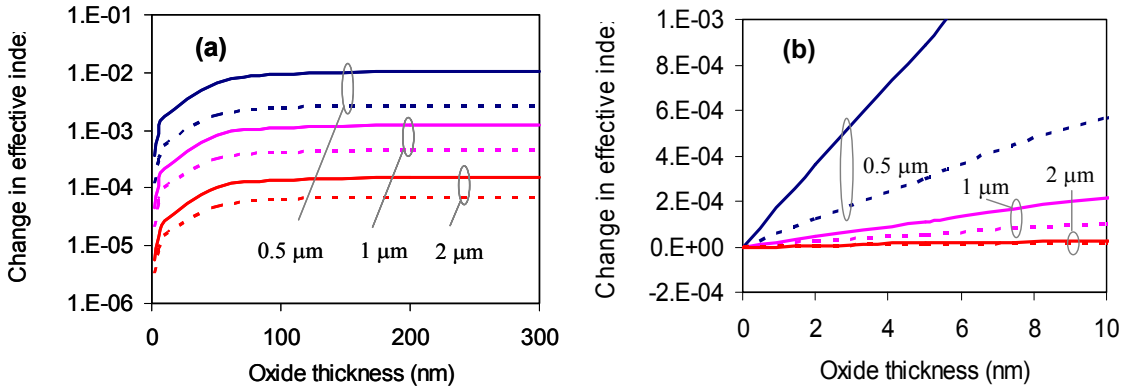

Fig. 2 Changes in the effective index as a function of the upper oxide cladding thickness t_c, in slab waveguides with silicon thickness H of 0.5, 1 and 2 μm, respectively. TM polarization: solid lines, TE polarization: dashed lines. (a) Logarithmic scale, (b) linear scale for thicknesses typical for native oxides.

3. BIREFRINGENCE: GEOMETRICAL EFFECTS

There are three main categories of SOI-based waveguides, i.e. slab, strip and ridge waveguides, as illustrated in Fig. 1. In the design of waveguide cross-sections, single mode like behavior and polarization insensitive operation are two requirements common to many types of waveguide components. Strip waveguides generally have a height H of less than 0.5 μm in order to limit the excitation of higher order modes. Such waveguides possess a high degree of polarization dependence that the appropriate approach for polarization management is beyond the scope of this work. Discussions on this topic can be found elsewhere.[25] Here we focus on ridge waveguides as shown in Fig. 1(c). It has been demonstrated through numerical simulations that ridge waveguides behave as single-mode devices when the following constraints are met.[26]

$$\frac{W}{H} \le 0.3 + \frac{r}{\sqrt{1-r^2}}, \qquad r = \frac{h}{H}, \tag{1a}$$

$$r \ge 0.5, \tag{1b}$$

where h is the slab height in the etched sections, W and H are the ridge width and height, respectively (see Fig. 1(c)). The restriction of Eq. (1b) is imposed because for $r \ge 0.5$, the effective index of the fundamental 'vertical mode' in the etched slab regions becomes larger than the effective index of all vertical high order modes in the ridge. Therefore all modes other than the fundamental mode in the ridge become 'leaky', and eventually dissipate after a sufficiently long propagation distance. In the original investigation, a propagation distance of 2 mm was used to verify the single mode like behavior in waveguides with a height H of 4 μm.[26]

Later publications applied the similar approach, and used the beam propagation method (BPM) or other beam propagators to study these criteria.[27-30] The conditions in Eq. (1) were investigated for waveguides with rectangular and trapezoidal cross-sections, and were claimed to be generally valid. The key consideration is that the higher order modes are 'leaky enough', so that only the fundamental mode remains in the waveguide after a sufficiently long propagation distance. Relatively large core sizes were studied. The propagation distances were often set to several millimeters and varied considerably between research groups. It was shown recently that certain higher order modes persist a very long propagation length.[31] In state-of-the-art devices, total propagation distances of several millimeters are common. It is difficult to establish universal criteria to determine the required loss for the higher order modes over a defined propagation distance to deem a waveguide 'single-mode'. Eq. (1) provides a useful guideline for designing single mode like waveguides, but does not serves as a rigorous condition.

It is also known that higher order modes have much larger radiation loss than the fundamental mode for a given bend radius, and waveguide bends can therefore be used as a mode-filtering mechanism.[32] In device designs, the single mode requirement should be dealt with more pragmatically, depending on the particular device configuration and the applications. With these arguments, we have extended our discussions on birefringence control over a wider range of waveguide cross-section profiles, some of which may not satisfy the conditions set forth in Eq. (1).

The propagation phase of an optical mode in a waveguide is

$$\varphi = \frac{2\pi n_{eff}\, z}{\lambda_0} \tag{2}$$

where n_{eff} is the effective index of the optical mode for the TE or TM polarizations, z is the propagation distance, λ_0 is the free-space wavelength and is taken as 1550 nm unless otherwise specified. When the TM and TE modes are not degenerate, a birefringence $\Delta n_{eff} = n_{eff}^{TM} - n_{eff}^{TE}$ arises. The corresponding wavelength shift between TM and TE polarizations due to the birefringence Δn_{eff} is

$$\Delta\lambda \approx -\frac{\Delta n_{eff}}{n_{eff}}\lambda_0 \tag{3}$$

For a change of 10^{-3} in the effective index n_{eff}, a phase change of $\pi/2$ results after propagation distance of 390 μm (assuming $n_{eff} \sim 3.45$). For a birefringence Δn_{eff} of 10^{-3}, the corresponding wavelength shift is 0.4 nm. Depending on the device configuration and the performance specifications, these levels of variations are often unacceptable. A high precision of control in the effective index and a minimum level of birefringence ($<10^{-4}$) is often required, particularly for telecommunication applications.

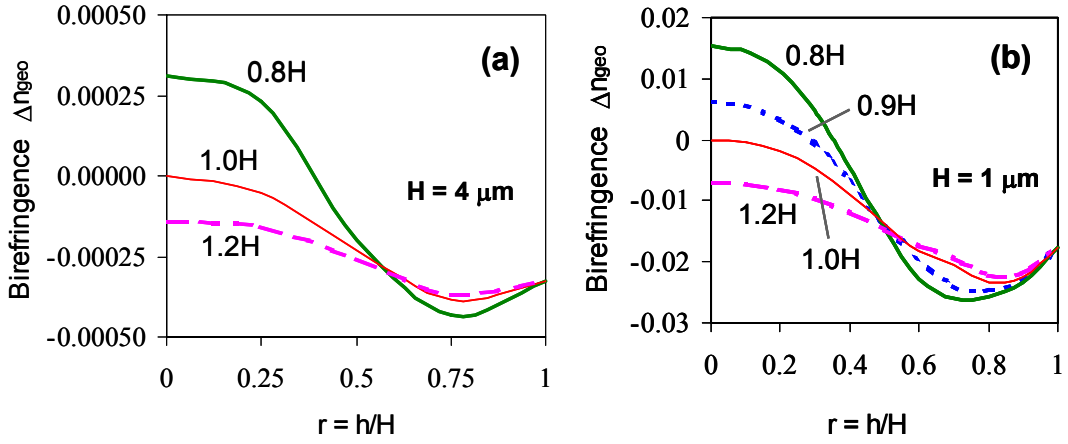

Fig. 3 Geometrical birefringence Δn_{geo} as a function of the ridge aspect ratio r, defined as the ratio between the height h of the etched slab section, and the total ridge height H, for different ridge width W as indicated in the figures. (a) H = 4 μm, (b) H=1 μm.

The birefringence consists of contributions from geometrical anisotropy Δn_{geo} and stress-induced birefringence Δn_s, and the total modal birefringence is $\Delta n_{eff} = \Delta n_{geo} + \Delta n_s$. The cross-section profile is the predominant factor controlling the waveguide modal effective index n_{eff}^{TM} and n_{eff}^{TE}. We first examine how the waveguide cross-section geometries affect the fundamental mode effective indices and the birefringence. In the discussions to follow, we assume that the lower cladding layer is 0.37 μm throughout the text to emulate our experimental condition. The upper oxide cladding thickness is assumed to be 0.5 μm in this section, and only the geometrical effects are discussed. For the range of the Si thickness discussed here, the optical field does not penetrate outside the cladding oxide layers into the air or the Si substrate, as shown in section 2. When the effects of the stress are considered in section 4, the upper cladding thickness may be varied. The refractive index of the materials are taken as n=3.476 for Si and n=1.444 for SiO_2 at the wavelength of 1550 nm. Modal indices are obtained using a commercial finite element mode solver. In slab waveguides, Δn_{geo} is always negative ($n_{eff}^{TM} < n_{eff}^{TE}$), and its magnitude increases rapidly with reducing core thickness H (on the order of 10^{-5} to 10^{-2} for H=5 μm to 1 μm). In strip waveguides shown in Fig. 1(b), the birefringence is zero when the cross-section is a square:

$$W=H \tag{4}$$

In ridge waveguides, Δn_{geo} changes with the etch depth D. Fig. 3 shows the dependence of Δn_{geo} with the ratio r = h/H, for rectangular waveguides of varying widths and ridge heights of 1 μm and 4 μm, respectively. When W = H, $\Delta n_{geo} = 0$ is only obtained when the ridge is etched to the buried oxide, at which point the waveguide becomes a square strip (r = 0). To obtain the geometrical birefringence-free condition $\Delta n_{geo} = 0$ in a ridge waveguide, it is a pre-requisite that:

$$W < H \tag{5}$$

For large r (shallow etch), Δn_{geo} first decreases with increasing etch depth D (reducing r) from the value for the slab, since the waveguide is weakly confined and it behaves similar to a slab with a reduced thickness of rH. At deeper etch depths, the mode is more confined, and Δn_{geo} shifts toward positive values. For W < H and at a single point of r (for the range of waveguide widths studied here), the TE and TM modes become degenerate and $\Delta n_{geo} = 0$.

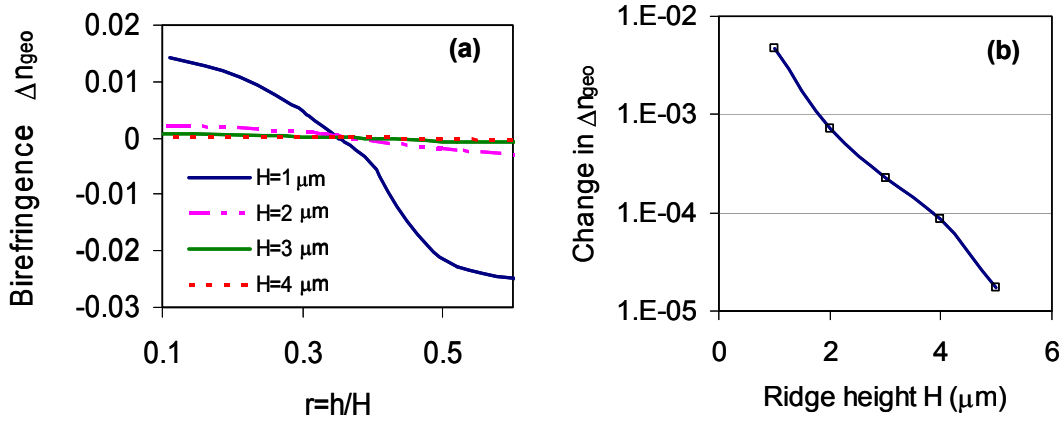

Fig. 4 (a) Geometrical birefringence Δn_{geo} as a function of the ridge aspect ratio r, for different ridge height H as indicated in the figures. The ridge width W is 80% of the ridge height H for all cases. (b) Change in the birefringence Δn_{geo} for a change of ±2.5%H in the etch depth D, as a function of the ridge height H. The data is extracted from Fig. 4(a) near the birefringence-free point.

It is apparent that the slope of the birefringence curves with respect to the etch depth near the birefringence-free point is steeper for narrower structures (smaller W). For large core size as the example of H = 4 μm shown in Fig. 3(a), the birefringence is generally low, and within a considerable range of values for r, Δn_{geo} is at acceptable levels ($<10^{-4}$). For small core size, however, only a very narrow range of r is usable. For H = 1 μm as shown in Fig. 3(b), near the

birefringence free point for W=0.8H, Δn_{geo} changes from -7.5×10^{-4} at r=0.35 to $+2.1\times10^{-4}$ at r = 0.36, which corresponds to a slope of ~ 2×10^{-3} per ±10 nm change in the etch depth. The dependence of Δn_{geo} on the aspect ratio r for different ridge height H is shown in Fig. 4(a) for waveguides with widths of 0.8H. The slope of the curves increases quickly with reducing H. Fig. 4(b) shows the change in Δn_{geo} near the birefringence-free point caused by a fluctuation in the etch depth by ± 2.5% H. Obviously, the requirement on the dimensional control becomes more and more stringent for microphotonic waveguides.

To further illustrate the dependence of waveguide birefringence on the ridge dimensions, Fig. 5(a) (dashed lines) shows the dependence of Δn_{geo} on the etch depth D for waveguides with H = 2.2 μm and width of 1.6 and 2.5 μm, respectively. Results for waveguides under stress (solid lines) will be discussed in section 4. For a given W, the polarization degeneracy (Δn_{geo} = 0) may be achieved at a single value of D. At the birefringence-free point for W = 1.6 μm, the change of Δn_{geo} with the fluctuation in the etch depth D is ~1.5×10^{-4} per ±10 nm. When W = 2.5 μm, Δn_{geo} is less sensitive to the fluctuations in the etch depth (~2×10^{-5} per ±10 nm at D = 1.5 μm), however the birefringence-free condition cannot be fulfilled. To reduce the birefringence below the level required for the state-of-the-art photonic devices (Δn_{eff} <10^{-4}) by adjusting the ridge aspect ratio W/D, dimension controls on the order of 10 nm are required for these rectangular waveguides.

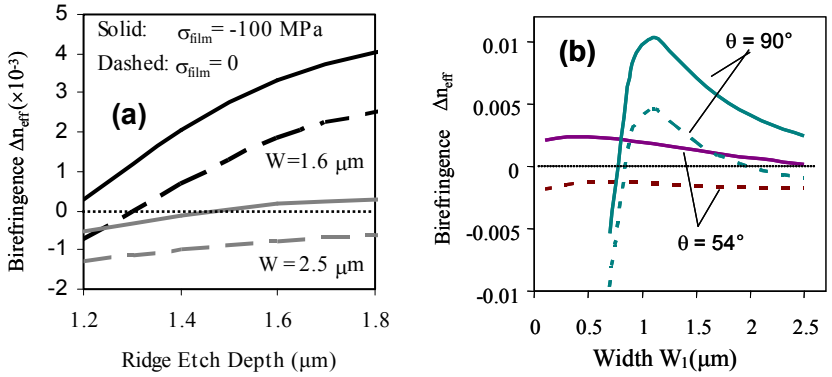

Fig. 5. (a) Calculated modal birefringence Δn_{eff} for waveguides with for H=2.2 μm. (a) Δn_{eff} in rectangular waveguides as a function of etch depth D, W = 1.6, 2.5 μm, t_c= 0.7 μm and σ_{film} = -100 MPa. (b) Δn_{eff} in rectangular (θ = 90º) and trapezoidal (θ = 54º) waveguides as a function of the top width W_1, for D = 1.5 μm, t_c =0.7 μm and σ_{film} = -300 MPa. The dashed curves show Δn_{geo} (i.e. in the absence of stress), the solid curves show Δn_{eff} including both the geometrical and stress-induced birefringence.

The effect of changing the waveguide width on Δn_{geo} is shown in Fig. 5(b), for two side wall angles 90° and 54°, which represent the profiles typically obtained by dry and anisotropic wet etchings, respectively. With reducing width, Δn_{geo} shifts towards positive values initially, until the waveguide is so narrow that the modes mainly reside in the etched slab section and the birefringence changes to negative values rapidly. Waveguide sidewall angles also strongly affect the mode properties, especially when the sidewall is near vertical. The birefringence of a trapezoidal ridge waveguide is less susceptible to changes in the ridge geometry (width and etch depth) as compared to a rectangular waveguide with similar cross-section area, which is evidenced by the data for a sidewall angle of 54° shown here. The geometrical birefringence, however, remains negative for the entire waveguide width range. For the rectangular waveguides, an optimal width can be found to satisfy the birefringence-free condition (zero birefringence at W~ 2 μm). More detailed discussions on the influence of sidewall angles can be found in previous publications.[21, 22, 25]

With the single-mode and birefringence-free requirements, it is important to be able to implement the designs using existing fabrication technologies. Using contact-print lithography for defining waveguides, waveguide width variations on the order of 100 nm can be expected. Using higher resolution methods such as e-beam direct write or deep UV steppers, dimensional control on the order of 10 nm is possible. Such techniques, however, are very expensive and are not widely available. Because it is difficult to precisely control the waveguide dimensions due to

limitations of the fabrication techniques, methods of controlling birefringence other than modifying waveguide geometries are preferred.

The fast changes in the effective indices and the birefringence with waveguide dimensions can be alleviated by using waveguides of wider widths. This, however, requires deeper etch for $\Delta n_{geo} = 0$, and this is in conflict with the single-mode requirement. For $W \geq H$, the $\Delta n_{geo} = 0$ condition does not exist at all. Waveguides with trapezoidal cross-sections are also less susceptible to dimensional fluctuations, however Δn_{geo} in these waveguides remains negative. We will discussion in section 4 on how to use stress-induced birefringence to mitigate this problem.

4. PHOTOELASTIC EFFECT AND THE STRESS-INDUCED BIREFRINGENCE

Apart from the geometrical effects discussed in section 2, a deposited or grown oxide layer usually is accompanied by the presence of a (compressive) stress in the oxide layer. This is due to the different thermal expansion coefficients of Si (3.6×10^{-6} K^{-1}) and oxide (5.4×10^{-7} K^{-1}), as well as intrinsic stress that may exist in the oxide film.

When a material is subjected to a stress, the material refractive index is altered due to the photoelastic effect. The stress-induced changes in the material refractive index are given by:[33, 34]

$$n_x - n_0 = -C_1\sigma_x - C_2(\sigma_y + \sigma_z) \quad (6a)$$
$$n_y - n_0 = -C_1\sigma_y - C_2(\sigma_z + \sigma_x) \quad (6b)$$

Here σ_i (i=x, y, z) is the stress tensor, n_i the material refractive index, n_0 the refractive index without stress, and C_1 and C_2 the stress-optic constants. If a stress (tensor) with axial anisotropy is imposed on an originally optically isotropic material, a material birefringence is induced:

$$n_y - n_x = (C_2 - C_1)(\sigma_y - \sigma_x) \quad (7)$$

Stress-optic constants of silicon and glass are listed in Table I, as well as those of GaAs for comparison.

Table I. Material constants of some materials

Material	λ (μm)	C_1 (10^{-12} Pa^{-1})	C_2 (10^{-12} Pa^{-1})
Si	1.15	-11.04	4.04
Glass	0.633	0.65	4.5
GaAs	1.15	-18.39	-10.63

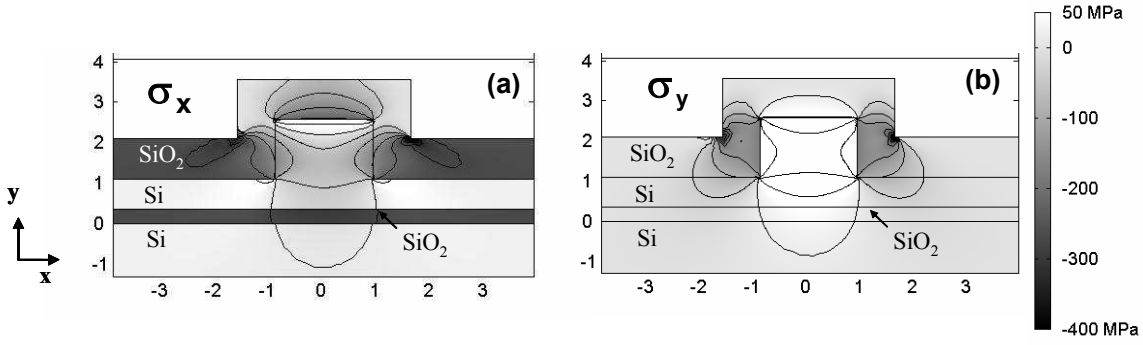

Fig. 6. Calculated stress distributions of a SOI waveguide in the (a) x-direction, and (b) y-direction. Here w=1.83 μm, D=1.47 μm, corresponding to the fabricated rectangular waveguides in Fig. 8(a), for t_c=1 μm and σ_{film}= -320 MPa. The dimensions are in microns.

In this section we use single waveguides with a height H of 2.2 μm to illustrate the typical characteristics of the stress-induced effects. Properties in multiple waveguides and waveguides with different ridge heights are discussed in section 6 and 7, respectively. Stress distributions in a SOI ridge waveguide calculated using the finite element method are shown in Fig. 6 (a) and (b) for SiO_2 upper and lower claddings under a compressive stress (σ_{film}= -320 MPa, where σ_{film} is the in-plane stress component in the uniform film far from the ridge), with the ridge dimensions described in the figure caption. Detailed analysis of the simulations methods were discussed in a previous publication.[22] We assumed the thickness of the oxide upper cladding film on the ridge sidewalls was 70% of that on the top, to simulate the depositions by plasma-enhanced chemical vapor depositions (PECVD) as used in our experiments.

The primarily in-plane (x) stress in the oxide film compresses the Si ridge, resulting in a compressive stress in the x-direction and a high tensile stress in the y-direction in the silicon core. These stress anisotropies cause a birefringence in the core and cladding materials. The stress in the core is mainly governed by the upper cladding, since the lower cladding exerts little force on the Si ridge due to the plane interface between the lower cladding and the core. We assumed the upper and lower claddings to have the same material properties, and the thickness of the lower cladding was a constant of 0.37 μm. For simplicity, the upper cladding will be referred to as the 'cladding'. Examining Eq. (6) and the stress-optic constants listed in Table I, we can conclude that for the Si core $n_x < n_0$ and $n_y > n_0$ when the upper cladding is under a compressive stress. These modifications in the material indices cause corresponding changes in the modal effective indices. As shown in Fig. 7(a), n_{eff}^{TM} increases with the oxide thickness and the stress magnitude, while n_{eff}^{TE} decreases. The absolute values of change are larger for TM mode than that for TE. For an appropriate combination of oxide thickness and the stress level, the TE and TM modes become degenerate and the birefringence-free condition is achieved.

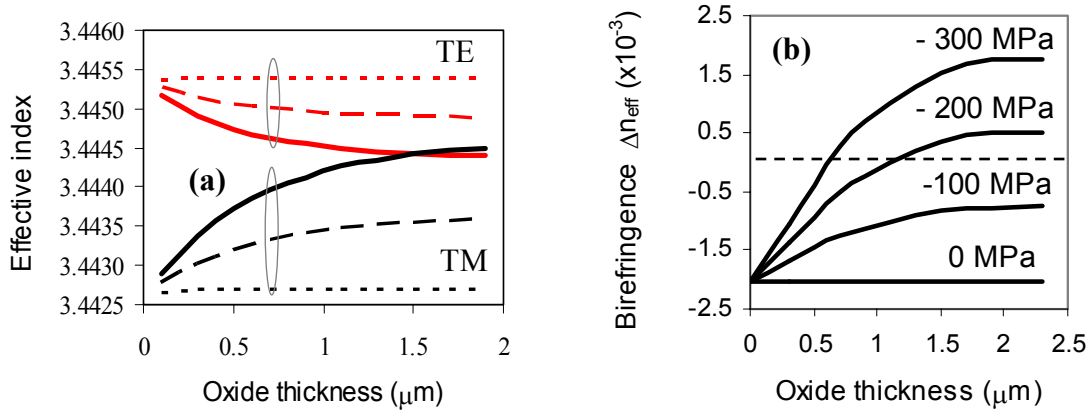

Fig. 7 (a) Effective index as a function of the oxide upper cladding thickness, for different cladding stress levels σ_{film} of 0 (dotted lines), -200 MPa (dashed lines, and -400 MPa (solid lines), respectively. (b) Δn_{eff} as a function of t_c and σ_{film} for waveguides with top width=1.1 μm, bottom width=3.8 μm and D=1.47 μm, corresponding to the trapezoidal waveguides in Fig. 8(a).

Fig. 7(b) shows the calculated dependence of total waveguide birefringence Δn_{eff} on the upper cladding thickness t_c for different values of the film stress σ_{film}. Total waveguide birefringence $\Delta n_{eff} = \Delta n_{geo} + \Delta n_s$, where Δn_{geo} and Δn_s are the geometrical and stress-induced birefringence respectively. For $\sigma_{film} = 0$, $\Delta n_{eff} = \Delta n_{geo}$, which has the characteristics discussed in section 3, and is only a weak function of t_c (once the mode is contained in the cladding). A cladding with compressive stress induces a positive shift in Δn_{eff}, which increases with the cladding thickness initially and eventually reaches a plateau. For the structure shown here, it gives a tuning range of 1.6×10^{-3} for σ_{film} of -300 MPa.

Evidently, there are two parameters which effectively control the stress-induced birefringence, namely the oxide thickness t_c and the stress level σ_{film}. Depending on the value of the geometrical birefringence Δn_{geo}, the magnitude of the total birefringence may be reduced, entirely compensated, or increased. It is straight forward to adjust the

oxide thickness experimentally. The stress level of the oxide can also be adjusted by varying the film deposition conditions. A cladding with tensile stress induces a negative shift in Δn_{eff}, should such a modification be desired. Silicon nitride (SiN) is one candidate that can serve such a purpose.

SOI platform offers very high refractive index contrast between the Si core and the oxide or air cladding. The stress-induced modifications to the refractive indices are orders of magnitude smaller than the refractive indices themselves, or the index contrast. Consequently, the stress-induced effects are only pertubative, while the cross-section geometry predominantly determines the mode properties of a waveguide. Simulations verify that the mode-mismatch loss between sections of waveguides with or without stress is negligible (<0.1 dB).

5. EXPERIMENTAL DEMONSTRATIONS

We have demonstrated the proposed birefringence control technique in AWG demultiplexers made on SOI substrates with a silicon thickness of 2.2 μm. The AWGs have 9 output channels with 200 GHz spacing and centered at 1550 nm. The arrayed waveguide gratings of order 40 were formed by 100 waveguides of width 2 μm. Both wet and dry etching were used to produce the waveguides, yielding ~54º and nearly vertical sidewall angles, respectively. Simulations were performed using measured waveguide dimensions. Upper cladding oxide films of different thicknesses were deposited at ~ 400ºC using PECVD, with a film stress of σ_{film} = –320 MPa in the slab films, measured from wafer bowing. These AWGs exhibited cross-talks of less than -25 dB between adjacent channels, indicating the effectiveness of higher order mode filtering by waveguide bends. The modal birefringence for waveguides forming the grating section was determined using $\Delta n_{eff} = n_g \Delta\lambda/\lambda_0$, where n_g is the waveguide group index, $\Delta\lambda=\lambda_{TM}-\lambda_{TE}$ is the polarization dependent wavelength shift between the central wavelengths for TM and TE polarizations, and λ_0 is the free-space operating wavelength. In calculating the birefringence, we assumed λ=1550 nm and n_g =3.65. Fig. 8 shows the calculated and measured dependence of $\Delta\lambda$ on the cladding thickness t_c, for both trapezoidal and rectangular waveguides. Calculated results agree well with experiments for both types of waveguides, showing that $\Delta\lambda$ can be modified over a 2 nm wide

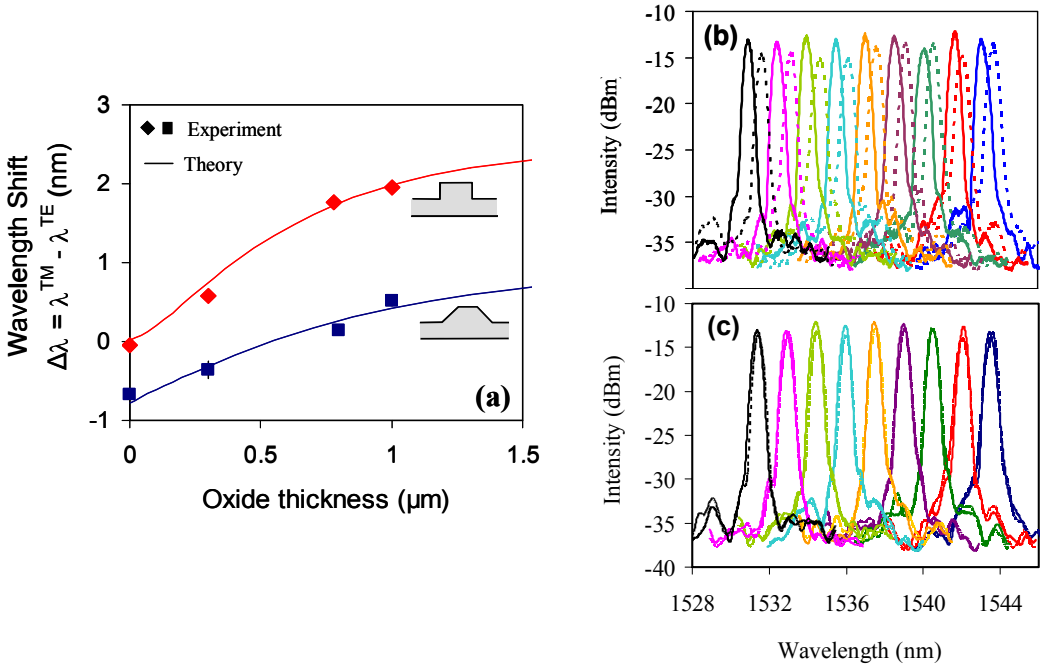

Fig. 8 (a) Dependence of Δn_{eff} with t_c, for AWGs fabricated using wet (trapezoidal W_1 = 1.85 μm and W_2 = 2.0) and dry (rectangular W_1 = 1.1 μm and W_2 = 3.8 μm) etching to D=1.47 μm and σ_{film}= -320 MPa; Spectra for an SOI AWG (b) without the oxide upper cladding, and (c) compensated using 0.6 μm thick SiO_2 claddings with σ_{film}= -320 MPa. TM (solid) and TE (dashed).

range by changing the cladding thickness. TE and TM spectra of an AWG with wet etched waveguides are shown in Fig 8 (b) and (c). The polarization dependent wavelength shifts across the spectrum were reduced to $\Delta\lambda < 0.04$ nm (corresponding to a modal birefringence of $\Delta n_{eff} < 1\times10^{-4}$) by depositing a 0.6 μm cladding oxide. Without the upper cladding layer, $\Delta\lambda$ was approximately -0.6 nm (corresponding to $\Delta n_{eff} \sim 1.3\times10^{-3}$). With the appropriately chosen oxide thickness and stress, the polarization sensitivity was virtually eliminated. Polarization dependent loss was also negligible in these devices.

The cladding stress level can also be adjusted by post-processing. Experiments on the birefringence tuning by modifying σ_{film} using thermal treatments were reported earlier.[35] Thermal anneals decreased the stress in the oxide films. The maximum modification in $\Delta\lambda$ was 0.2 nm by anneals at 650º C for up to 20 min, providing a practical method of post-process tuning.

6. MULTIPLE WAVEGUIDES

In the previous sections, we considered the effects of cladding stress in a single ridge waveguide. For the example shown in Fig. 6, we can see that the nonuniformity of the stress field extends several microns from the ridge center. In this section we examine the structures of two parallel waveguides with varying spacing. This is particularly of interest in devices such as directional couplers and ring-resonators where waveguides come in close proximity.

Fig 9(a) and (b) show the stress distributions in two waveguides with a separation of 1.2 μm, to simulate the situation in a directional coupler. The ridge height H is 2.2 μm, the width W is 1.5 μm and the etch depth is 1.1 μm. The cladding thickness is 0.7 μm, with 70% coverage on the sidewalls and σ_{film} of -108 MPa. The basic characteristics of the stress field are similar to that presented in Fig 6 (a) and (b). The primarily in-plane (x) stress in the oxide film compresses the Si ridges, resulted in a compressive stress in the x-direction and a tensile stress in the y-direction in the silicon cores. When in such close proximity, the modes in the waveguides are coupled and can be represented by the so-called super-modes of symmetric and anti-symmetric electric field distributions. The dependence of the super-mode effective indices on the ridge separation (distance from edge to edge) is shown in Fig. 10(b), with or without the influence of the cladding stress. For the data with no stress, the presence of the upper cladding oxide and the geometrical effect is still included.

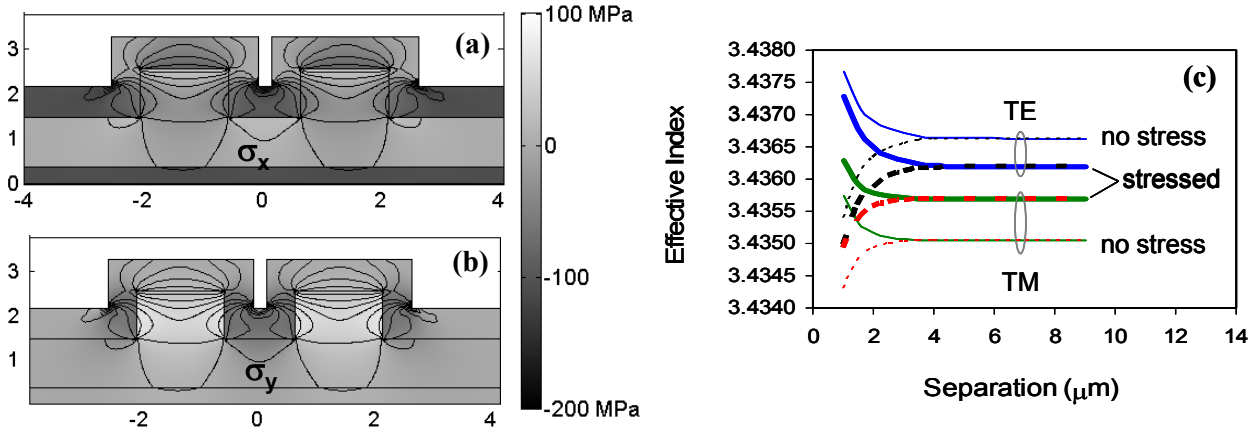

Fig. 9. Calculated stress distributions of two parallel SOI waveguides with H of 2.2 μm in the (a) x-direction, and (b) y-direction. The dimensions are in microns. Here waveguide width W is 1.5 μm, etch depth D is 1.1 μm, and the waveguide separation (edge to edge) is 1.2 μm, for t_c=0.7 μm and σ_{film}= -108 MPa. (c) Effective indices of the symmetric (solid lines) and the anti-symmetric (dashed lines) modes as a function of the ridge separation, for waveguides of the same dimensions as in (a).

When the two waveguides are sufficiently far apart, the symmetric and anti-symmetric modes are degenerate. With decreasing ridge separations, the index difference between the symmetric and anti-symmetric modes becomes larger, and the coupling length decreases. The cladding stress induces shifts for the TE and TM modes which are nearly constant for all the ridge separations. Similar to the single ridge case, the value of the shift is negative for TE and positive for TM, and they are of similar magnitude for the symmetric and anti-symmetric modes of the same polarization. For the waveguide separation range considered here, the maximum variation in the stress-induced changes is ~ 5×10^{-5}, while the separation causes changes on the order of 1.5×10^{-3}. The controlling factor for the coupling length is the waveguide separation. Therefore the effect of stress can be used as an adjustment constant to vary the birefringence, allowing the coupling characteristics to be optimized separately, as will be discussed in section 8.

7. SCALING WITH THE CORE SIZE

So far we have examined the characteristics of stress-induced effects for a ridge height of H=2.2 μm. These effects for different core sizes are studied in this section. Fig. 10 shows the evolution of the material birefringence (n_y-n_x) in the ridges of different height H but of the same aspect ratio (r=0.375), with 1 μm of oxide upper cladding and σ_{film} = -105 MPa. When the entire etched section is buried in the oxide ($t_c \geq D$), as for the case of H = 1 μm shown in Fig. 10(a), the Si core is under tensile stress and n_y-$n_x \geq 0$ for the entire ridge area. As the ridge height H increases relative to the oxide thickness t_c, to the point that part of the ridge is above the horizontal height of the cladding film ($t_c < D$), this portion of the core is actually stretched in the x-direction and compressed in the y-direction, while the portion 'sandwiched' between the in-plane cladding film is still under the tensile force, as shown for the case of H = 3 and 5 μm here. As long as the tensile stressed portion of the core has a significant overlap with the optical filed, a positive shift is induced in the birefringence. Shown in Fig. 11 is the dependence of stress-induced birefringence on the cladding thickness. For a given ridge height H and etch depth D, when the cladding thickness t_c increases, there is a larger portion of the core under the in-plane force ($t_c\times\sigma_{film}$) of the cladding, and the stress-induced birefringence Δn_s increases. When t_c approaches D, Δn_s approaches a maximum and saturates. For the same cladding thickness, a smaller Δn_s is induced for a larger core. Their saturation values, however, are of the same order of magnitude for all the ridge heights considered here, and it is ~ 10^{-3} for σ_{film} = -105 MPa. This is a significant effect on the birefringence, even with such a low stress film, and has to be taken into consideration in the design of SOI waveguide components.

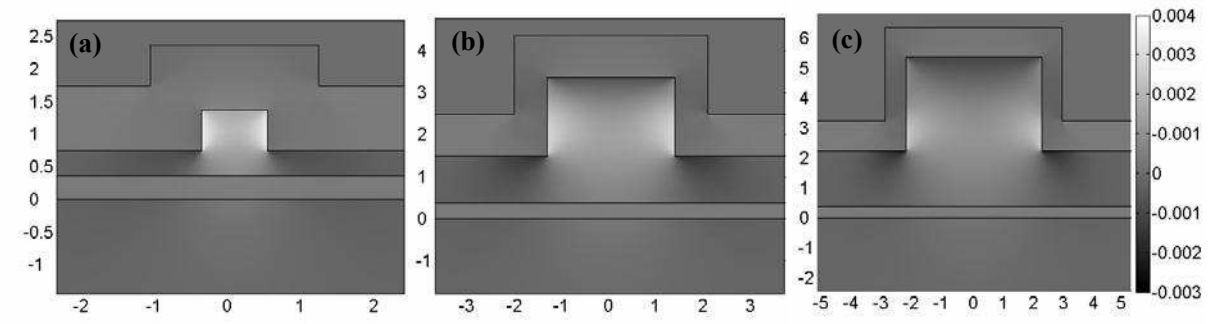

Fig. 10 Material birefringence (n_y-n_x) in SOI waveguides with a width of 0.9 H, and an aspect ratio r of 0.375, for ridge height H of (a) 1 μm, (b) 3 μm, and (c) 5 μm. The oxide thickness is 1 μm, with a stress σ_{film} of -105 MPa.

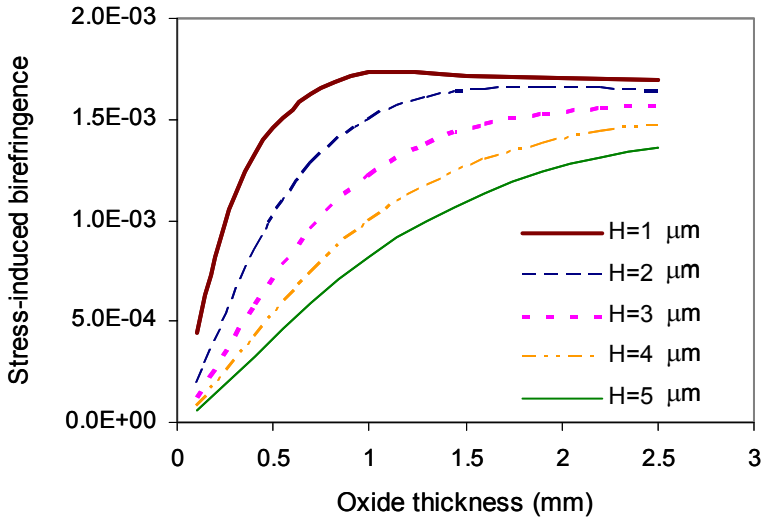

Fig. 11. Stress-induced modal birefringence Δn_s in SOI waveguides with a width of 0.9 H, and an aspect ratio r of 0.375, for ridge height H 1, 2, 3, 4, and 5 μm, respectively. The corresponding etch depths for these ridge heights are 0.625, 1.25, 1.875, 2.50, and 3.125 μm. Take note of the oxide thickness where Δn_s approaches a plateau. The oxide thickness is 1 μm, with a stress σ_{film} of -105 MPa.

8. DESIGN OPTIONS

As we have seen, stress-induced effects on the effective indices of the TE and TM modes and the associated birefringence are of significance for a wide range of SOI waveguide geometries commonly employed. Left unattended, this will lead to departures in device characteristics from the designed specifications. Fortunately, the use of cladding stress to correct the birefringence of a range of waveguide sizes allows a considerable degree of freedom in designing SOI waveguides to meet other performance criteria such as relaxed dimensional tolerance, reduced loss at waveguide bends, and improved coupler performance. Two examples are discussed in the following.

As discussed in section 3 and illustrated in e.g. Fig. 5, waveguide aspect ratios determine the sensitivity of birefringence to ridge dimensions. Wider waveguides (W>H) are less sensitive to dimension fluctuations (e.g. etch depth change as shown in Fig. 5(a). However, a negative Δn_{geo} persists. By using a compressively stressed cladding with σ_{film} = -100 MPa, the geometrical birefringence can be balanced by the stress-induced birefringence, as shown by the solid curve for W of 2.5 μm guides. Improved process latitude can be obtained. For this example, the dependence of Δn_{geo} on the etch depth D is relaxed from 1.5×10^{-4} per ±10 nm for W = 1.6 μm, to 2×10^{-5} per ±10 nm for W = 2.5 μm. It is shown in Fig. 7(b) that Δn_s reaches a plateau once the oxide thickness is comparable to the etch depth. It is preferable to operate near the plateau, so that Δn_s only varies with the oxide thickness t_c very gradually for better control. We have found that Δn_s is proportional to the stress magnitude σ_{film} for a given t_c. The stress-induced birefringence Δn_s required to compensate for the Δn_{geo} is approximately 1×10^{-3}. Therefore to limit Δn_{eff} within $\pm5\times10^{-5}$, control in the stress level of ±5% is required, which is achievable in fabrications. Trapezoidal waveguides offer similar advantages in lower susceptibility to dimensional changes, even when taking into account the profile variations along a waveguide bend associated with anisotropic wet etching, which is a common method for producing trapezoidal waveguides.[25] Similar approaches in stress-engineering can be applied, and the experimental demonstration is presented in section 5. In fact, a range of thickness and stress level combinations can be used to satisfy the birefringence-free requirement for various waveguide profiles with non-zero Δn_{geo}.

With stress engineering, the birefringence can be corrected as a final step using deposition of the appropriate cladding. The cladding correction technique is also amenable to post fabrication birefringence tuning by annealing to modify the film stress, or adding /removing a small amount of cladding.[35]

In the case of directional couplers or ring resonators, the challenge is to balance the constraints set by the coupling length and bend radius which determine the free-spectral-range (FSR), the bend loss, the equal coupling for the TE and TM polarizations, as well as the birefringence-free requirement. The challenges of meeting these constrains in producing polarization insensitive ring-resonators were discussed recently.[19] Using stress engineering, some requirements can be better accommodated. Consulting the data shown in Fig. 3 and Fig. 9(c), we can contemplate the options made available. For example, a wider waveguide with a negative Δn_{geo} can be chosen to give relaxed dimensional tolerance and better fiber to waveguide coupling efficiency. A shallower etch depth can be used to better match the single mode condition, and to reduce the waveguide coupling length, yielding larger FSR. The negative Δn_{geo} can be balanced by the proper combination of cladding thickness and stress level, while maintaining similar waveguide coupling properties.

9. SUMMARY

High index contrast (HIC) waveguide platforms such as silicon-on-insulator (SOI) and Si_3N_4 in silica allow a significant reduction in component foot-print, which is further facilitated by decreasing the core size. This opens new opportunities for integrated, high-functionality photonic circuits for applications in data transmission, telecommunication, optical analysis and diagnostics. To implement microphotonic devices as a viable technology, several challenges must be overcome. One of the fundamental challenges is the control of polarization sensitivity, which becomes increasingly difficult to manage as the waveguide dimensions shrink.

We have presented the characteristics of the geometrical and stress-induced birefringence, for SOI ridge waveguides with heights H ranging from 1-5 μm. Waveguide width and etch depth determine the geometrical birefringence Δn_{geo}. For waveguides with H of 5 μm, Δn_{geo} is on the order of 1×10^{-4} for a considerable range of waveguide profiles, and the traditional method of controlling the aspect ratio is effective. As the ridge height decreases, waveguides are more strongly confined by the ridge boundaries, and Δn_{geo} becomes increasingly sensitive to the ridge dimensions. For H of 2 μm and W of 1.6 μm, a fluctuation in the etch depth of ± 50 nm causes a change of ~ 8×10^{-4} in Δn_{geo}. Not only Δn_{geo} becomes more difficult to control to a low level, the birefringence-free requirement also interferes with other design considerations. For example, a shallower etch depth is required to maintain single-mode like behavior, which demands a narrower waveguide width in order to obtain $\Delta n_{geo} = 0$, and that in turn deteriorate the fiber-waveguide coupling and exacerbate the dimensional sensitivity. The minimum bend radius usable is also compromised. These are some of the dilemma facing SOI-based microphotonics.

Stress is inherent in multi-layer planar waveguide systems, and the stress modifies the refractive indices of the constituting layers through the photoelastic effect. The stress-induced modifications to the effective indices in SOI waveguides are mainly controlled by the stress level and the thickness of the upper oxide cladding. Due to the high index contrast, oxide thickness of 0.3 μm is sufficient to isolate the mode from the surrounding environment for the waveguides considered in this work, while the stress field extends for several microns. Thicknesses greater than 0.3 μm is effective in modifying the stress-induced effects. With commonly found stress levels σ_{film} in oxide films (-100 MPa to -400 MPa), and a thickness comparable to the etch depth, stress-induced birefringence Δn_s can reach the order of 10^{-3} for all ridge heights considered. Using this effect, we demonstrate that stress engineering is an effective tool to modify or eliminate birefringence in SOI waveguide devices, for a wide range of waveguide cross-section geometries and dimensions. Decoupled from birefringence constraints, waveguide geometries can then be optimized for other performance criteria. Wider waveguides or trapezoidal waveguides may be chosen to relax the tolerance to dimensional fluctuations, and still satisfy the birefringence-free condition by balancing out Δn_{geo} with the appropriate Δn_s. Wider waveguides or shallower etch depth may be chosen to optimized the performance in a directional coupler or a ring resonator, while compensating the Δn_{geo} with the stress-induced effect.

Since the effect of a SiO_2 cladding on mode shape is negligible, there is little mode mismatch loss or PDL associated with the junction between waveguide sections with and without claddings. Therefore it is possible to apply tailored cladding patches at discrete locations in a planar waveguide circuit with little insertion loss penalty. Although the initial experimental demonstration of this technique has been in compensating the birefringence in AWG demultiplexers, oxide stress can be applied in many situations including polarization correction of ring resonators, waveguide grating filters, Mach-Zehnder interferometers. Cladding stress can also be used to create a specific birefringence for polarization control devices including polarization filters and splitters.

10. REFERENCES

1. V. R. Almeida, C. Barrios, R. Panepucci and M. Lipson, Nature **431**, p. 1081, 2004.
2. A. Liu, R. Jones, L. Liao, D. Samara-Rubio, D. Rubin, O. Cohen R. Nicolaescu and M. Paniccia, Nature **427**, 615 (2004).
3. O. Boyraz, B. Jalali, Optics Express **12**, p. 5269 (2004).
4. J. Liu, J. Yu, S. Chen and J. Xia, Optics Communications, www.sciencedirect.com (2004).
5. P. Cheben, A. Bogdanov, A. Delâge, B. Lamontagne, S. Janz, M.-J. Picard, E. Post, and D.-X. Xu, SPIE Proc. **5644,** paper 17 (2004).
6. R. R. Whiteman, A. P. Knights, D. George, I. E. Day, A. Vonsovici, A. A. House, G. F. Hopper and M. Asghari, "Recent process in the design, simulation and fabrication of small cross-section silicon-on-insulator VOAs", Proc. SPIE **4997**, pp. 146-156 (2003).
7. L. Pavesi and D. Lockwood, Eds. "Silicon Photonics", Berlin: Springer Verlag (2004).
8. T. Shoji, T. Tsuchizawa, T. Watanabe, K.Yamada and H. Morita, 'Low loss mode size converters from 0.3 μm square Si wire waveguides to single mode fibers", Electron. Lett., **38**(25), 1669-1670 (2002).
9. P. Cheben, D.-X. Xu, S. Janz and A. Delâge, "Scaling down photonic waveguide devices on the SOI platform", SPIE 5117, pp. 147-156 (2003).
10. S. Janz, P. Cheben, A. Delage, B. Lamontagne, M.-J. Picard, D.-X. Xu, K.-P. Yap, and W.N. Ye, "Silicon-based integrated optics – waveguide technology to microphotonics", Materials Research Society Symposium Proceedings **832** (in press, 2005).
11. A. Delâge, S. Janz, D.-X. Xu, D. Dalacu, B. Lamontagne, and A. Bogdanov, SPIE Proc. **5577,** Photonics North 2004 (in press, 2004).
12. G. Masanovic, V.M.N. Passaro, and G.T. Reed, IEEE Phot. Technol. Lett. **15**, 1395 (2003).
13. V.R. Almeida, R.R. Panepucci, and M. Lipson, Opt. Lett. **28**, 1302 (2003).
14. K.K. Lee, D.R. Lim, H.-C. Luan, A. Agarawal, J. Foresi, and L.C. Kimmerling, Appl. Phys. Lett. **77**, 1617 (2000).
15. K.K. Lee, D.E. Lim, L.C. Kimmerling, J. Shin, and F. Cerrina, Opt. Lett. **26**, 1888 (2001).
16. D.-X. Xu, P. Cheben, D. Dalacu, A. Delˆage, S. Janz, B. Lamontagne, M. Picard, and W. N. Ye, "Eliminating the birefringence in siliconon-insulator ridge waveguides using the cladding stress," Opt. Lett. **29**, 2384 (2004).
17. L. Vivien, S. Laval, B. Dumont, S. Lardenois, A. Koster, and E. Cassan: "Polarization-independent single-mode rib waveguides on silicon on insulator for telecommunications wavelengths", Opt. Commun. 210, pp. 43-49 (2002).
18. D Dai and S. He, "Analysis of the birefringence of a silicon-on-insulator rib waveguide", Applied Optics 43(5), 1156-1161 (2004).
19. G. T. Reed, S. P. Chan, W. Headley, V. M. N. Passaro, A. Liu and M. Paniccia, "Polarisation independent devices in small SOI waveguides", Proceedings of the IEEE/LEOS Group VI Photonics Conference, Paper FB5, Hong Kong (CD, 2004).
20. B. Jalali, R. Claps, D. Dimitropoulos and V. Raghunathan, "Light generation, amplification, and wavelength conversion via stimulated Raman scattering in silicon microstructures", in "Silicon Photonics", L. Pavesi and D. Lockwood, Eds.Berlin: Springer Verlag (2004).
21. D.-X. Xu, P. Cheben, S. Janz, and D. Dalacu, "Control of SOI waveguide polarization properties for microphotonic applications", Proc. 5th CLEO-Pacific Rim, TU3I-(8)-5. Taipei, Taiwan, Dec. 15-19, 2003.
22. W. N. Ye, D.-X. Xu, , S. Janz, P. Cheben, M.-J. Picard, B. Lamontagne and N.G. Tarr, "Birefringence control using stress engineering in silicon-on-insulatr (SOI waveguides:, J. Lightwave Technology (in press, 2005).

23. A. Kilian, J. Kirchhof, B. Kuhlow, G. Przyrembel and W. Wischmann, "Birefringence free planar optical waveguide made by flame hydrolysis deposition (FHD) through tailoring of the overcladding", J. Lightwave Technol. **18**(2), pp. 193-198 (2000).
24. C. Nedler, E. K. Wildermuth, M. Lanker, W. Hunziker, and H. Melchior, "Polarization insensitive, low-loss, low-crosstalk wavelength multiplexer modules", IEEE J. Sel. Topics in Quantum Electronics **5**(5), pp. 1407-1412 (1999).
25. D.-X. Xu, J.-M. Baribeau, P. Cheben, D. Dalacu, A. Delâge, B. Lamontagne, S. Janz, M.-J. Picard, and W. N. Ye, "Prospects and challenges for microphotonic waveguide components based on Si and SiGe", ECS Proc. **2004-07**, 619-633 (2004).
26. R. A. Soref, J. Schmidtchen, and K. Petermann, "Large single-mode waveguides in GeSi-Si and Si-on-SiO2," IEEE J. Quantum Electron., **27**, pp. 1971–1974, 1991.
27. S. Pogossian, L. Vescan and A. Vonsovici, "The single-mode condition for semiconductor rib waveguides with large cross section', J. Lightwave Technol. **16**(10), 1851-1853 (1998).
28. A. G. Rickman, G. T. Reed and F. Namarva, :Silicon-on-insulator optical rib waveguide loss and mode characteristics", J. Lightwave Technol. **12**(10), 1771-1776 (1994).
29. O. Powell, "Single-mode condition for silicon rib waveguides", J. Lightwave Technol. **20**(10), 1851-1855 (2002).
30. J. Xia and J. Yu, "Singel-mode condition for silicon rib waveguides with trapezoidal cross-section", Optics Communications, www.sciencedirect.com (2003).
31. J. Lousteau, D. Furnuss, A. B. Seddon, T. M. Benson, A. Vukovicand P. Sewell, "The single mode condition for silicon-on-insulator optical rib waveguides with large cross-section", J. Lightwave Technol. **22**(8), 1923-1929 (2004).
32. M. R. T. Pearson, A. Bezinger, A. Delâge, J. W. Fraser, S. Janz, P. E. Jessop, and D.-X. Xu, "Arrayed waveguide grating demultiplexers in silicon-on-insulator," Proc. SPIE **3593**, pp. 11–18, 2000.
33. M. Huang, "Stress effects on the performance of optical waveguides, 'Inter. J. Solids and Structures, **40**, pp. 1615–1632, 2003.
34. T. S. Narasimhamurty, "Photoelastic and electro-optic properties of crystals", Plenum Press, New York (1981).
35. D.-X. Xu, P. Cheben, D. Dalacu, S. Janz, M.-J. Picard, N. G. Tarr, and W. N. Ye, "Control and compensation of birefringence in SOI waveguides", Proc. 16th LEOS, WM4, p. 590. Tucson, Arizona. October 26-30, 2003.